Journal of Contaminant Hydrology 126 (2011) 301–314

Contents lists available at SciVerse ScienceDirect

Journal of Contaminant Hydrology

journal homepage: www.elsevier.com/locate/jconhyd

Transport of biocolloids in water saturated columns packed with sand: Effect of grain size and pore water velocity

Vasiliki I. Syngouna, Constantinos V. Chrysikopoulos *

Department of Civil Engineering, Environmental Engineering Laboratory, University of Patras, Patras 26500, Greece

ARTICLE INFO

Article history:
Received 14 February 2011
Received in revised form 11 July 2011
Accepted 24 September 2011
Available online 02 October 2011

Keywords:
Coliphages
Bacteria
Sand
Grain size
Pore water velocity
Transport
Deposition
Mathematical modelling

ABSTRACT

The main objective of this study was to evaluate the combined effects of grain size and pore water velocity on the transport in water saturated porous media of three waterborne fecal indicator organisms (*Escherichia coli*, MS2, and ΦX174) in laboratory-scale columns packed with clean quartz sand. Three different grain sizes and three pore water velocities were examined and the attachment behavior of *Escherichia coli*, MS2, and ΦX174 onto quartz sand was evaluated. The mass recoveries of the biocolloids examined were shown to be highest for *Escherichia coli* and lowest for MS2. However, no obvious relationships between mass recoveries and water velocity or grain size could be established from the experimental results. The observed mean dispersivity values for each sand grain size were smaller for bacteria than coliphages, but higher for MS2 than ΦX174. The single collector removal and collision efficiencies were quantified using the classical colloid filtration theory. Furthermore, theoretical collision efficiencies were estimated only for *E. coli* by the Interaction-Force-Boundary-Layer, and Maxwell approximations. Better agreement between the experimental and Maxwell theoretical collision efficiencies were observed.

1. Introduction

Groundwater may be accidentally contaminated with infective human enteric viruses from human and animal sewage through wastewater discharges, sanitary landfills, septic tanks, and agricultural practices (Sim and Chrysikopoulos, 2000) or by artificial groundwater recharge, which is often used to reverse the rapid depletion of aquifers (Anders and Chrysikopoulos, 2005; Chrysikopoulos et al., 2010; Masciopinto et al., 2008). To predict the presence of pathogens in water and wastewater, microorganisms known as indicator organisms (e.g. bacteria *Escherichia coli*, and coliphages MS2 and ΦX174), which are commonly associated with fecal contamination, are monitored.

Many studies examining the interaction of microorganisms with soil, sand, gravel or other model granular materials have been conducted using laboratory-scale columns under well-controlled environmental conditions (Hijnen et al., 2005; Jin et al., 1997; Keller et al., 2004; Ryan et al., 1999). Theoretical and experimental studies have examined the effect of pore water solution chemistry (Bolster et al., 2001; Sadeghi et al., 2011), fluid velocity (Chrysikopoulos and Sim, 1996; Hendry et al., 1999), matrix structure, moisture content, temperature, grain size (Anders and Chrysikopoulos, 2006, 2009; Bolster et al., 2001; Sim and Chrysikopoulos, 2000; Torkzaban et al., 2008; Vasiliadou et al., 2011), and presence of surface coatings (Bolster et al., 2001; Ryan et al., 1999) on microbial transport and retention in porous media. Quartz sand, either clean or coated, as well as glass beads have all been employed as model granular materials in such studies. Some researchers have also investigated the transport of microorganisms through columns packed with excavated soils or undisturbed soil cores, and provided valuable information regarding the influence of soil chemistry and matrix structure on microbial transport and retention (Banks et al., 2003; Walshe et al., 2010). Although a large number of studies focusing on various factors that affect microbial transport have been published over the past two

* Corresponding author. Tel.: +30 2610 996531; fax: +30 2610 996573.
E-mail address: gios@upatras.gr (C.V. Chrysikopoulos).

0169-7722/$ – see front matter © 2011 Elsevier B.V. All rights reserved.
doi:10.1016/j.jconhyd.2011.09.007

decades, it is not fully understood yet how these factors concurrently affect biocolloid transport in porous media.

Grain size and water velocity are known to impact colloid transport in porous media; however to our knowledge, their combined and synergistic effects on biocolloid transport and retention in porous media has not been previously explored. This study improves our understanding of how various combinations of grain sizes and pore water velocities impact the transport and attenuation of *E. coli*, MS2, and ΦX174 in laboratory columns packed with 'clean' saturated quartz sand. The collision efficiencies of the three biocolloids examined were estimated theoretically and experimentally using relatively low specific discharge velocity ($0.16 \le q \le 0.51$ cm/min), and the factors that control biocolloid deposition were discussed.

2. Materials and methods

2.1. Bacterial and coliphage suspensions

Although there exists a large variety of *Escherichia* (*E.*) *coli* bacterial strains with large diversity in cell properties and transport behavior, in this study, the bacterial strain *E. coli* CN-13 (ATCC 700609), a well-characterized, Gram-negative, typical representative of the coliform bacteria, was used. *E. coli* cells are motile rod shaped with approximate dimensions of 0.6 μm in width and 2 μm in length (Maki et al., 2000), or with an equivalent spherical diameter of 1.21 μm. To provide a uniform inoculum for each experiment, a stock culture was cultivated in 50 mL of tryptic soy broth medium for 6 h to early stationary phase, harvested by centrifugation for 10 min at $5000 \times g$ and washed twice with sterile phosphate buffered saline (PBS) solution (1.2 mM NaCl, 0.027 mM KCl, and 0.10 mM Na_2HPO_4) to remove nutrients. Finally, the pellet was suspended in PBS solution in a manner similar to that described by Foppen and Schijven (2005) and stored at 4 °C until application. Aliquots were taken to count the bacteria. Bacteria were suspended and diluted in PBS solution at pH = 7 to concentrations of $1.94 \pm 0.06 \times 10^8$ colony-forming units per milliter (CFU/mL). The *E. coli* concentration was determined using optical density measurements (at 410 nm) with a UV-visible spectrophotometer (UV-1100, Hitachi). The bacterial cell concentrations (plate colonies) were determined using a standard spectrophotometer calibration curve.

Coliphages MS2 and ΦX174 were chosen because of their structural resemblance to many human enteric viruses and because they have been studied as surrogates for human enteric viruses in numerous investigations. The coliphage MS2 is a F-specific, single-stranded RNA phage with 31% nucleic acid content, whose host bacterium is *E. coli* (ATTC 15597-B1); whereas, the coliphage ΦX174 is an icosahedral, single-stranded DNA phage with 26% nucleic acid content, whose host bacterium is *E. coli* (ATTC 13706-B1). The MS2 particle diameter ranges from 24 to 26 nm; whereas, the ΦX174 particle diameter ranges from 25 to 27 nm. The protein coat of MS2 is relatively hydrophobic and sensitive to interfacial forces that appear to cause its inactivation; whereas, ΦX174 has hydrophilic protein coat (Shields, 1986). Both coliphages were assayed by the double-layer overlay method (Adams, 1959), where 0.1 mL of the appropriate host bacterium and 0.1 mL of a diluted virus sample solution were mixed in a centrifuge tube. The mixture was combined with molten soft-agar medium (4.5 mL) maintained at 45 °C in a tube and poured onto a petri dish containing solid agar medium. The plates were solidified for 10 min and incubated overnight at 37 °C. Viable virus concentrations were determined by counting the number of plaques in each host lawn and reported as plaque-forming units per milliter (PFU/mL). With the exception of the first few early and late breakthrough samples, for all samples collected, only dilutions that resulted in the range of 20–300 plaques per plate were accepted for quantification. All virus concentrations reported represent the average of two replicate plates. Coliphages, MS2 and ΦX174, were suspended and diluted in PBS solution at pH = 7 to concentrations of 10^3–10^6 PFU/mL. Furthermore, batch inactivation experiments were conducted in the presence of sand to determine the inactivation rate coefficient for MS2 4.2×10^{-5} min^{-1} and ΦX174 2.0×10^{-5} min^{-1}.

2.2. Chloride analysis

Chloride, in the form of potassium chloride, was chosen as the nonreactive tracer for the transport column experiments. The nonreactive tracer solution was prepared with 0.01 M KCl in PBS solution. It should be noted that alkali halides are the most commonly used salts for subsurface fluid tracing owing to a minimal effect on solution ionic strength (I_S) (Chrysikopoulos, 1993). Chloride concentrations were measured using ion chromatography (ICS-1500, Dionex Corp., Sunnyvale, CA).

2.3. Column packing material

Quartz sand of various sizes was used as packing material in the experimental columns. The sand was purchased directly from the manufacturer (Filcom Filterzand & Grind) and sieved into various size distributions. In this study three size distributions were used: (a) coarse (1.18–1.7 mm or sieve No 16), (b) medium (0.425–0.600 mm or sieve No 40), and (c) fine (0.150–0.212 mm or sieve No 100). The various uniformity coefficients, $C_u = d_{60}/d_{10}$, were estimated to be $C_u = 1.19$, 1.21, 1.2 for fine, medium, coarse sand, respectively. The chemical composition of the sand reported by the manufacturer was: 96.2% SiO_2, 0.15% Na_2O, 0.11% CaO, 0.02% MgO, 1.75% Al_2O_3, 0.78% K_2O, 0.06% SO_3 and 0.46% Fe_2O_3, 0.03% P_2O_5, 0.02% BaO, and 0.01% Mn_3O_4. The total organic carbon (% TOC) content, measured by the Walkley–Black method (i.e., chemical oxidation of the organic fraction) (Black, 1965), was found equal to 0.08 ± 0.04% for the coarse, and 0.1 ± 0.1% for both medium and fine sand fractions. Prior to the experiments, the sand fractions were cleaned with 0.1 M HNO_3 (70%) for a 3 h time period to remove surface impurities (e.g., iron hydroxide and organic coatings) that could promote physicochemical deposition of the biocolloids, rinsed with deionized water, then soaked in 0.1 M NaOH for a 3 h time period, and rinsed again with deionized water. After the cleaning steps, the sand was dried in an oven at 105 °C, and then stored in screw cap sterile beakers until use in the column experiments.

2.4. Column experiments (PBS experiments)

The glass columns (2.5 cm diameter and 30 cm length) were packed wet with sand under vibration to minimize any layering or air entrapment. The porosity of the sand column was determined by standard procedures. Prior to each experiment, the

packed column was equilibrated by pumping 10 pore volumes of the background PBS solution through the column at a constant volumetric discharge rate of Q = 2.5, 1.5 and 0.8 mL/min, corresponding to specific discharge or approach velocities of q = 0.51, 0.31 and 0.16 cm/min, respectively. It should be noted that the specific discharge velocities employed in this work are quite low and thus representative of slow sand filter and field conditions. A suspension of each biocolloid of the same background PBS solution was pumped for 3 pore volumes at the same Q followed by 5 pore volumes of biocolloid-free PBS solution. The apparatus used for the biocolloid transport experiments are shown in Fig. 1.

3. Theoretical developments

3.1. Transport modeling

One-dimensional biocolloid transport in homogeneous, water saturated porous media with first-order attachment (or filtration) and inactivation is governed by the following partial differential equation (Sim and Chrysikopoulos, 1995):

$$\frac{\partial C(t,x)}{\partial t}+\frac{\rho}{\theta}\frac{\partial C^*(t,x)}{\partial t} = D\frac{\partial^2 C(t,x)}{\partial x^2}-U\frac{\partial C(t,x)}{\partial x}-\lambda C(t,x)-\lambda^*\frac{\rho}{\theta}C^*(t,x) \quad (1)$$

where C is the concentration of biocolloids in suspension; C* is the concentration of biocolloids attached on the solid matrix; D is the hydrodynamic dispersion coefficient (Bear, 1979):

$$D=\alpha_L U+D_e \quad (2)$$

where α_L is the longitudinal dispersivity, $D_e = D/\tau^*$ is the effective molecular diffusion coefficient ($\tau^* \geq 1$ is the tortuosity coefficient, and D is the molecular diffusion coefficient); U is the interstitial velocity; ρ is the bulk density of the solid matrix; λ is the transformation rate constant of biocolloids in solution (e.g., inactivation of suspended viruses); λ* is the transformation rate constant of attached biocolloids; θ is the porosity of the porous medium; and t is time. The rate of biocolloid attachment onto the solid matrix is described by the following first-order equation (Sim and Chrysikopoulos, 1998, 1999):

$$\frac{\rho}{\theta}\frac{\partial C^*(t,x)}{\partial t}=k_c C(t,x)-k_r\frac{\rho}{\theta}C^*(t,x)-\lambda^*\frac{\rho}{\theta}C^*(t,x) \quad (3)$$

where k_c is the attachment rate constant, and k_r is the detachment rate constant.

For a semi-infinite one-dimensional porous medium in the presence of a continuous source of biocolloids, the appropriate initial and boundary conditions are:

$$C(0,x)=0 \quad (4)$$

$$-D\frac{\partial C(t,0)}{\partial x}+UC(t,0)=\begin{cases} UC_0 & 0<t\leq t_p \\ 0 & t>t_p \end{cases} \quad (5)$$

$$\frac{\partial C(t,\infty)}{\partial x}=0 \quad (6)$$

where C_0 is the source concentration and t_p is the duration of the solute pulse. Condition (4) establishes that there is no initial biocolloid concentration within the one-dimensional porous medium. The constant flux boundary condition (5) implies a biocolloid concentration discontinuity at the inlet. The downstream boundary condition (6) preserves concentration continuity for a semi-infinite system. The analytical solution to the governing biocolloid transport Eq. (1) in conjunction with relationship (3), subject to conditions (4)–(6) has been derived by Sim and Chrysikopoulos (1995) as follows:

$$C(t,x)=\begin{cases} \Omega(t,x) & 0<t\leq t_p \\ \Omega(t,x)-\Omega\left(t-t_p,x\right) & t>t_p \end{cases} \quad (7)$$

where

$$\begin{aligned}\Omega(t,x)=&\frac{C_0U}{D^{1/2}}\exp\left[\frac{Ux}{2D}\right]\left\{\int_0^t\int_0^\tau He^{-H\tau}J_0\left[2(B\xi(\tau-\xi))^{1/2}\right]\right.\\ &\cdot\left\{\frac{1}{(\pi\xi)^{1/2}}\exp\left[\frac{-x^2}{4D\xi}+\left(H-A-\frac{U^2}{4D}\right)\xi\right]\right.\\ &-\frac{U}{2D^{1/2}}\exp\left[\frac{Ux}{2D}+(H-A)\xi\right]\\ &\left.\cdot\operatorname{erfc}\left[\frac{x}{2(D\xi)^{1/2}}+\frac{U}{2}\left(\frac{\xi}{D}\right)^{1/2}\right]\right\}d\xi d\tau\\ &+e^{-Ht}\int_0^t J_0\left[2(B\xi(t-\xi))^{1/2}\right]\\ &\cdot\left\{\frac{1}{(\pi\xi)^{1/2}}\exp\left[\frac{-x^2}{4D\xi}+\left(H-A-\frac{U^2}{4D}\right)\xi\right]\right.\\ &-\frac{U}{2D^{1/2}}\exp\left[\frac{Ux}{2D}+(H-A)\xi\right]\\ &\left.\left.\cdot\operatorname{erfc}\left[\frac{x}{2(D\xi)^{1/2}}+\frac{U}{2}\left(\frac{\xi}{D}\right)^{1/2}\right]\right\}d\xi\right\}.\end{aligned} \quad (8)$$

where $A=k_c+\lambda$, $B=k_c k_r\theta/\rho$, $H=(k_c\theta/\rho)+\lambda^*$ (Sim and Chrysikopoulos, 1998, p.92), J_0 is the Bessel function of the first kind of zeroth order, and ξ and τ are dummy integration variables. Note that the various model parameters can be estimated by fitting the analytical solution Eq. (7) to the experimental data with the nonlinear least squares regression program COLLOIDFIT (Sim and Chrysikopoulos, 1995).

3.2. Moments

The biocolloid concentration breakthrough data obtained at location x = L were analyzed by the absolute temporal moments:

$$m_n(x)=\int_0^\infty t^n C_i(x,t)dt \quad (9)$$

where the subscript n = 0, 1, 2, … indicates the order of the moment, and subscript i indicates *E. coli*, MS2, and ΦX174. The zeroth absolute temporal moment, m_0, quantifies the total mass in the concentration breakthrough curve; the first absolute moment, m_1, describes the mean residence time; and second absolute temporal moment, m_2, describes

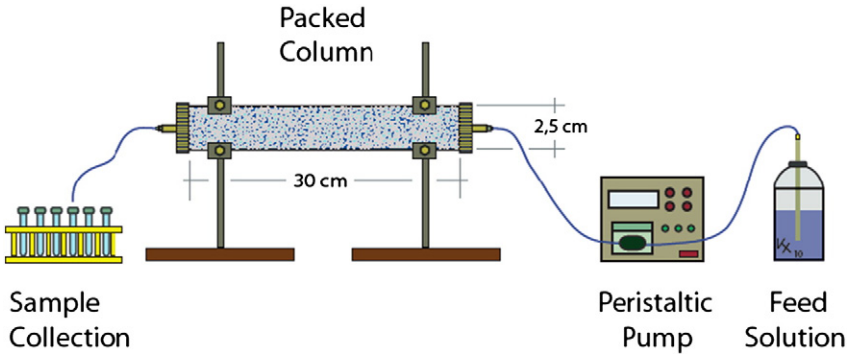

Fig. 1. Schematic illustration of the experimental apparatus.

the degree of spreading of the concentration breakthrough curve. Also, the normalized temporal moments are defined as (James and Chrysikopoulos, 2011):

$$M_n(x)=\frac{m_n(x)}{m_0(x)}=\frac{\int_0^\infty t^n C_i(x,t)dt}{\int_0^\infty C_i(x,t)dt} \tag{10}$$

The first normalized temporal moment, M_1, characterizes the center of mass of the concentration breakthrough curve and defines the mean breakthrough time or average velocity. The second normalized temporal moment, M_2, characterizes the spreading of the breakthrough curve. Worthy to note is that the ratio $M_{1(i)}/M_{1(t)}$ indicates the degree of velocity enhancement of biocolloid i relative to the conservative tracer. If this ratio is less than one, there exists velocity enhancement of biocolloid transport. If this ratio is greater than one there exists biocolloid retardation. Furthermore, the mass recovery, M_r, of the tracer or the suspended particles is quantified by the following expression:

$$M_r(L)=\frac{m_0(L)}{C_{i_0}t_p}=\frac{\int_0^\infty C_i(L,t)dt}{\int_0^{t_p} C_i(0,t)dt} \tag{11}$$

where L is the porous medium length.

3.3. Colloid filtration theory

Classical colloid filtration theory (CFT) was used to quantitatively compare the microbial and viral attachment onto quartz sand. CFT assumes that the removal of particles is described by first-order kinetics with a spatially and temporally constant rate of particle deposition, and the concentrations of retained particles decrease log-linearly with distance. However, recent studies (Tong and Johnson, 2007; Tufenkji and Elimelech, 2004) have suggested that colloid retention decreased hyper-exponentially with distance, suggesting that the attachment rate coefficient is not constant. In the absence of straining, which is defined as the trapping of particles in pores that are too small to pass through, this hyper-exponential deviation from CFT could be attributed to the concurrent existence of both favorable and unfavorable colloidal interactions with collector surfaces (Tufenkji and Elimelech, 2004). Particle deposition is termed favorable in the absence of repulsive interaction energies, whereas unfavorable deposition refers to the case where repulsive colloidal interactions predominate.

The dimensionless collision efficiency, α (the ratio of the collisions resulting in attachment to the total number of collisions between particles and collector grains), was calculated from each biocolloid breakthrough curve by the Rajagopalan and Tien (1976) model:

$$\alpha=-\frac{2d_c\ln(1-RB)}{3(1-\theta)\eta_0 L} \tag{12}$$

where d_c is the average collector grain diameter, η_0 is the dimensionless single-collector removal efficiency for favorable deposition (in the absence of double layer interaction energy), and RB is the ratio of the biocolloid mass recovery, $M_{r(i)}$, in the outflow relative to that of the tracer, $M_{r(t)}$:

$$RB=\frac{M_{r(i)}}{M_{r(t)}} \tag{13}$$

It should be noted that CFT is valid for clean-bed filtration where it is assumed that deposited biocolloids do not influence subsequent deposition of biocolloids. The relation between k_c and d_c was defined as (Anders and Chrysikopoulos, 2005; Harvey and Garabedian, 1991)

$$\frac{k_c}{\alpha}=\frac{3(1-\theta)}{2d_c}U\eta_0 \tag{14}$$

where the interstitial velocity is defined as

$$U=\frac{q}{\theta} \tag{15}$$

The single-collector removal efficiency for favorable deposition is obtained from the following correlation (Tufenkji and Elimelech, 2004):

$$\eta_0=2.4A_s{}^{1/3}N_R{}^{-0.081}N_{Pe}{}^{-0.715}N_{vdW}{}^{0.052}+0.55A_sN_R{}^{1.675}N_A{}^{0.125}+0.22N_R{}^{-0.24}N_G{}^{1.11}N_{vdW}{}^{0.053} \tag{16}$$

where A_s is a porosity-dependent flow parameter defined as

$$A_S=\frac{2\left(1-\varepsilon_\theta^5\right)}{2-3\varepsilon_\theta+3\varepsilon_\theta^5-2\varepsilon_\theta^6} \tag{17}$$

where $\varepsilon_\theta = (1-\theta)^{1/3}$, N_R is the relative size number:

$$N_R = \frac{d_p}{d_c} \tag{18}$$

N_{Pe} is the Peclet number:

$$N_{Pe} = \frac{d_c q}{D} \tag{19}$$

N_{vdW} is the van der Waals number:

$$N_{vdW} = \frac{A_{123}}{k_B T} \tag{20}$$

N_A is the attraction number:

$$N_A = \frac{N_{vdw}}{N_R N_{Pe}} \tag{21}$$

N_G is the gravity number:

$$N_G = \frac{{d_p}^2\left(\rho_p - \rho_f\right)g}{18\mu_w q} \tag{22}$$

where the bulk diffusion coefficient is described by the Stokes–Einstein equation as

$$D = \frac{k_B T}{3\pi\mu_w d_p} \tag{23}$$

$A_{123} = 7.5\times10^{-21}$ (kg·m^2/s^2) is the complex Hamaker constant of the interactive media (biocolloid-water-sand) (Murray and Parks, 1978), $k_B = 1.38\times10^{-23}$ (kg·m^2)/(s^2·K) is the Boltzman constant, T = 298 K is the fluid absolute temperature, d_p is the particle diameter (2.5×10^{-8} m for MS2, 2.6×10^{-8} m for ΦX174 and 1.2×10^{-6} m for *E. coli*), ρ_p is the particle density (1420 kg/m^3 for MS2 (Walshe et al., 2010), 1600 kg/m^3 for ΦX174 (Feng et al., 2006), and 1080 kg/m^3 for *E. coli* (Klaus et al., 1997)), $\rho_f = 999.7$ kg/m^3 is the fluid density, $\mu_w = 8.91\times10^{-4}$ kg/(m·s) is the absolute fluid viscosity, and g = 9.81 m/s^2 is the acceleration due to gravity.

3.4. Theoretical collision efficiency

Two approaches are available for the estimation of the theoretical collision efficiency, α_{th}. The first method is using the interaction-force boundary-layer (IFBL) approximation, which assumes that biocolloids are attached to the primary minimum, Φ_{min1}, and that α_{th} depends upon the probability of biocolloids crossing the primary maximum, Φ_{max1}, of the intersurface potential energy, Φ_{tot} (see Fig. 2) (Spielman and Friedlander, 1974):

$$\alpha_{th} = \left(\frac{\beta}{\beta+1}\right)S(\beta) \tag{24}$$

where $S(\beta)$ is a slightly varying monotonic dimensionless function that describes the collection of Brownian particles onto a spherical collector (a tabulation of $S(\beta)$ is given by Spielman and Friedlander (1974)), and β is a dimensionless sticking parameter given by

$$\beta = \frac{1}{3}(2)^{1/3}\Gamma\left(\frac{1}{3}\right)A_S{}^{-1/3}\left(\frac{D}{q r_p}\right)^{1/3}\left(\frac{\lambda_\beta r_p}{D}\right) \tag{25}$$

where Γ is the gamma function, r_p is the particle radius, and λ_β is the surface reaction rate coefficient describing adhesion and is given by the ratio of the diffusive rate of transfer of particles onto the collector surface to the overall rate of adhesion taking into account biocolloid mobility reduction due to hydrodynamic interactions (Dahneke, 1975):

$$\lambda_\beta = \frac{D}{\int_0^\infty\left[\left(1+\frac{r_p}{h}\right)e^{\Phi_{tot}/k_B T}-1\right]dh} \tag{26}$$

where h is particle-collector separation distance. Note that at the limit $\beta\to\infty$, the value of the surface reaction rate coefficient vanishes, $S(\beta)\to1$.

For a particle with radius r_p and a flat plate (collector with radius r_c and $r_p < r_c$) separated by a distance h the required variable Φ_{tot} is the sum of the van der Waals, Φ_{vdW}, double layer, Φ_{dl}, and Born, Φ_{Born}, potential energies (Loveland et al., 1996):

$$\Phi_{tot}(h) = \Phi_{vdW}(h) + \Phi_{dl}(h) + \Phi_{Born}(h) \tag{27}$$

The Φ_{vdW} for sphere-plate interactions was calculated with the following expression (Gregory, 1981):

$$\Phi_{vdw}(h) = -\frac{A_{123} r_p}{6h}\left[1+\left(\frac{14h}{\lambda_w}\right)\right]^{-1} \tag{28}$$

where $\lambda_w \approx 10^{-7}$ m is the characteristic wavelength of the sphere-plate interaction. This expression is quite accurate for short distances (up to 20% of the particle radius). The Φ_{dl} for sphere-plate geometry was calculated with the expression (Hogg et al., 1966)

$$\Phi_{dl}(h) = \pi\varepsilon_r\varepsilon_0 r_p\left[2\Psi_p\Psi_c\ln\left(\frac{1+e^{-\kappa h}}{1-e^{-\kappa h}}\right)+\left(\Psi_p^2+\Psi_c^2\right)\ln\left(1-e^{-2\kappa h}\right)\right] \tag{29}$$

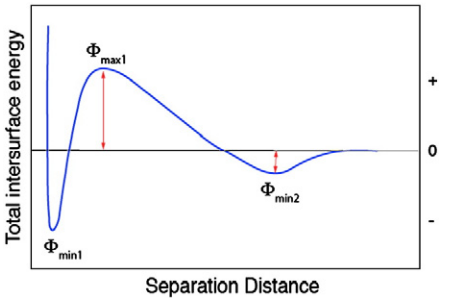

Fig. 2. Definition sketch of the total intersurface energy, Φ_{tot}, versus particle-collector separation distance, showing the primary minimum, Φ_{min1} (deep energy "well" located close to the collector surface), the primary maximum, Φ_{max1} (energy barrier to attachment and detachment), and the secondary minimum, Φ_{min2} (shallow energy "well" located some distance away from the collector surface).

where $\varepsilon_r = \varepsilon/\varepsilon_0$ is the dimensionless relative dielectric constant of the suspending liquid, ε is the dielectric constant of the suspending liquid, ε_0 is the permittivity of free space, Ψ_p is the surface potential of the particle, and Ψ_c is the surface potential of the collector (sand) and κ is inverse of the diffuse layer thickness, known as the Debye–Huckel parameter:

$$\kappa = \left[\frac{2I_s A_N 1000e^2}{\varepsilon_r \varepsilon_0 k_B T}\right]^{1/2} \tag{30}$$

where I_s is the ionic strength, $N_A = 6.02\times10^{23}$ 1/mol is Avogadro's number, and $e = 1.602\times10^{-19}$C is the elementary charge. Sometimes the electrokinetic zeta potentials (ζ) are used instead of the surface potentials for the calculation of Φ_{dl} in Eq. (29). The Φ_{Born} was estimated by the relationship (Ruckenstein and Prieve, 1976)

$$\Phi_{Born}(h) = \frac{A_{123}\sigma^6}{7560}\left[\frac{8r_p + h}{\left(2r_p + h\right)^7} + \frac{6r_p - h}{h^7}\right] \tag{31}$$

where σ (m) is the Born collision parameter. Note that Φ_{Born} can easily be neglected if $h > 1$ nm.

The second method for the calculation of α_{th} is based on the assumption that biocolloids are deposited in the secondary minimum, Φ_{min2} (note that the energy in the secondary minimum is negative, see Fig. 2), and can move back into the bulk liquid if their thermal energy (Brownian motion) is sufficiently high (Hahn and O'Melia, 2004). Assuming that the velocities of small biocolloids in a liquid at thermal equilibrium follow a Maxwell distribution, α_{th} is directly related to the Maxwell–Boltzmann distribution of the kinetic energies as follows (Simoni et al., 1998)

$$\begin{aligned}\alpha_{th(min2)} &= 1 - \int_{-\Phi_{min2}}^{\infty} f(E_k)dE_k \\ &= \int_0^{-\Phi_{min2}} f(E_k)dE_k\end{aligned} \tag{32}$$

where E_k is the kinetic energy of a biocolloid:

$$E_k = \frac{1}{2}m_p v_p^2 \tag{33}$$

where m_p is the mass of a biocolloid particle, v_p is the velocity of a biocolloid in the secondary minimum, and the Maxwell–Boltzmann distribution function is just a transformation of the Maxwell speed distribution function that describes how particles are distributed in regard to their kinetic energies (Bueche, 1975):

$$f(E_k)dE_k = 2\left[\frac{E_k}{\pi(k_B T)^3}\right]^{1/2}\exp\left[-\frac{E_k}{k_B T}\right]dE_k \tag{34}$$

Shen et al. (2007) assumed that colloids in the secondary minimum with kinetic energies larger than the total energy barrier (Φ_{max1}-Φ_{min2}) can also be deposited in the primary minimum, Φ_{min1} (see Fig. 2), and expressed α_{th} by considering both primary and secondary minimum deposition:

$$\begin{aligned}\alpha_{th} &= \alpha_{th(min1)} + \alpha_{th(min2)} \\ &= \int_{\Phi_{max1}-\Phi_{min2}}^{\infty} f(E_k)dE_k + \int_0^{-\Phi_{min2}} f(E_k)dE_k \\ &= 1 - \int_{-\Phi_{min2}}^{\Phi_{max1}-\Phi_{min2}} f(E_k)dE_k\end{aligned} \tag{35}$$

Hereafter, the α_{th} estimation by Eqs. (32) and (35) will be referred to as MA1 and MA2, respectively.

4. Results

4.1. Transport experiments

The normalized chloride breakthrough data for the coarse sand and three different specific discharge velocities are presented in Fig. 3. Similar results were observed (not shown) for the medium and fine sand. The dispersion coefficient was estimated for each sand column by fitting the analytical solution Eq. (7) with $k_c = k_r = \lambda = \lambda^* = 0$ to the experimental breakthrough chloride concentrations. The fitted dispersion coefficients and the corresponding longitudinal dispersivities calculated according to Eq. (2), using $D = 1\times10^{-9}$ m^2/s for chloride ions at 25 °C (Robinson and Stokes, 1959), are listed in Table 1.

The normalized *E. coli* breakthrough data are presented in Fig. 4 together with the fitted model predictions. In order to satisfactory match the breakthrough data collected in this study with simulated concentration histories requires knowledge of

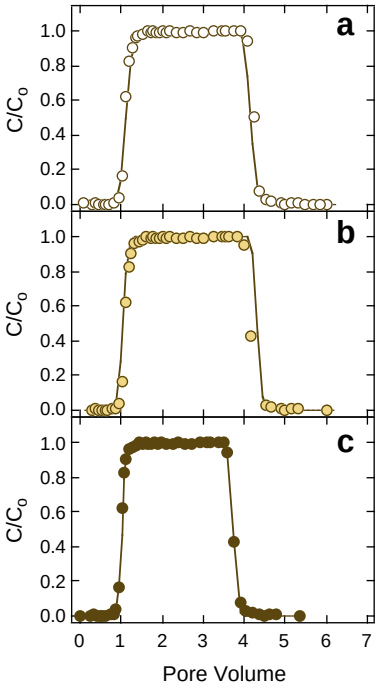

Fig. 3. Tracer breakthrough data (symbols) and fitted mathematical model predictions (solid curves) for specific discharge velocities of (a) 0.16, (b) 0.31, and (c) 0.51 cm/min in water-saturated columns packed with coarse sand.

Table 1
Calculated parameter values.

q (cm/min)	pH effluent	d_c (μm)	C_0 PFU/mL (viruses) CFU/mL (bacteria) mmol/mL (tracer)	ρ_b (g/cm^3)	θ	U (cm/min)	D (cm^2/min)	α_L (cm)	$M_{1(i)}/M_{1(t)}$	M_r (%)	η_0	α
ΦX174												
0.51	7.20	1118–1700	4.4×10^3	1.69	0.43	1.17	0.51	0.44	0.83	100	0.046	0.0001
0.51	7.20	425–600	3.4×10^3	1.69	0.42	1.21	0.29	0.24	0.92	100	0.089	0.0000
0.51	7.20	150–212	4.1×10^3	1.69	0.39	1.31	0.53	0.51	0.87	82.7	0.172	0.0007
0.31	7.02	1118–1700	2.6×10^6	1.72	0.41	0.76	0.30	0.42	0.96	100	0.053	0.0001
0.31	6.90	425–600	1.8×10^6	1.72	0.4	0.78	0.16	0.21	0.84	88.2	0.103	0.0023
0.31	7.07	150–212	1.7×10^6	1.69	0.41	0.76	0.08	0.11	0.93	100	0.196	0.0000
0.16	7.43	1118–1700	2.4×10^3	1.72	0.43	0.39	0.11	0.26	0.82	95.4	0.082	0.0032
0.16	7.00	425–600	2.8×10^3	1.72	0.4	0.4	0.03	0.08	0.86	100	0.166	0.0000
0.16	6.99	150–212	2.2×10^3	1.69	0.41	0.39	0.34	0.79	0.83	100	0.314	0.0000
MS2												
0.51	7.19	1118–1700	4.2×10^5	1.69	0.4	1.3	1.33	1.29	0.88	88.9	0.049	0.0107
0.51	7.08	425–600	4.7×10^5	1.72	0.42	1.21	1.06	1.01	0.98	71.6	0.096	0.0056
0.51	7.22	150–212	2.95×10^5	1.65	0.36	1.41	1.17	0.93	0.86	100	0.165	0.0000
0.31	7.06	1118–1700	7.3×10^3	1.72	0.41	0.76	0.49	0.83	1.05	87.0	0.055	0.0135
0.31	6.89	425–600	7.3×10^3	1.72	0.39	0.79	0.30	0.40	0.87	96.5	0.109	0.0006
0.31	7.23	150–212	7.3×10^3	1.68	0.43	0.72	0.21	0.30	0.94	91.9	0.194	0.0003
0.16	7.18	1118–1700	7.3×10^3	1.72	0.4	0.4	0.71	1.48	0.81	70.2	0.090	0.0205
0.16	7.40	425–600	2×10^4	1.72	0.42	0.38	0.67	1.89	0.98	65.4	0.164	0.0051
0.16	6.99	150–212	3.25×10^3	1.69	0.4	0.4	0.50	1.46	0.92	43.5	0.331	0.0017
E. coli												
0.51	7.08	1118–1700	1.9×10^8	1.71	0.39	1.31	0.67	0.56	0.93	100	0.003	0.0216
0.51	7.21	425–600	1.94×10^8	1.77	0.39	1.31	0.42	0.32	0.93	95.3	0.005	0.0149
0.51	7.19	150–212	1.88×10^8	1.72	0.41	1.24	0.44	0.36	0.89	100	0.009	0.0001
0.31	6.99	1118–1700	1.88×10^8	1.7	0.39	0.79	0.18	0.23	0.93	100	0.004	0.0015
0.31	7.15	425–600	1.97×10^8	1.72	0.43	0.72	0.07	0.09	0.86	100	0.006	0.0004
0.31	7.23	150–212	2×10^8	1.69	0.44	0.71	0.04	0.06	0.88	100	0.011	0.0001
0.16	7.32	1118–1700	1.98×10^8	1.73	0.39	0.41	0.09	0.22	0.85	95.9	0.006	0.0357
0.16	7.24	425–600	2×10^8	1.76	0.39	0.41	0.03	0.08	0.91	94.5	0.010	0.0103
0.16	7.19	150–212	1.88×10^8	1.71	0.39	0.41	0.12	0.29	0.88	96.2	0.020	0.0013
Tracer Cl^-												
0.51	7.02	1118–1700	0.01	1.76	0.42	1.21	0.20	0.167		99.7		
0.51	6.81	425–600	0.01	1.72	0.43	1.20	0.21	0.173		100		
0.51	6.76	150–212	0.01	1.72	0.39	1.31	0.24	0.180		99.7		
0.31	7.08	1118–1700	0.01	1.76	0.42	0.74	0.16	0.209		100		
0.31	6.94	425–600	0.01	1.72	0.43	0.72	0.15	0.211		100		
0.31	6.81	150–212	0.01	1.72	0.39	0.79	0.15	0.190		100		
0.16	6.89	1118–1700	0.01	1.76	0.42	0.38	0.08	0.197		99.5		
0.16	7.13	425–600	0.01	1.72	0.43	0.37	0.06	0.169		99.8		
0.16	6.76	150–212	0.01	1.72	0.39	0.41	0.08	0.193		100		

the various k_c values, which were calculated by using Eq. (14) and previously calculated η_0 and α values. The parameters D, and k_r, were estimated by fitting the analytical solution Eq. (7) to the experimental *E. coli* breakthrough concentrations using the values of ρ θ U, k_c listed in Table 1, and assuming that $\lambda=\lambda^*=0$. The fitted k_r values were negligible and the fitted D values are listed in Table 1. The first normalized temporal moment (average velocity), $M_{1(i)}$, was calculated using Eq. (10) for each breakthrough curve. Furthermore, the ratio of the first normalized temporal moment of *E. coli* to that of Cl^- was computed for each breakthrough curve and the results are listed in Table 1. For all cases considered the ratio $M_{1(i)}/M_{1(t)}$ was smaller than one, which indicated that the velocity of *E. coli* is enhanced by 7%–15%. Early breakthrough of colloids has been reported in numerous theoretical and experimental studies (Abdel-Salam and Chrysikopoulos, 1995; Keller et al., 2004; Sinton et al., 2000; Vasiliadou and Chrysikopoulos, 2011). The M_r values, listed in Table 1, were calculated using Eq. (11) and indicate that there was no significant *E. coli* retention by the packed column. Slight attachment of *E. coli* onto the quartz sand was observed at the lowest q. However, no distinct relationships between M_r or $M_{1(i)}/M_{1(t)}$ and q or d_c could be established from the data listed in Table 1.

The parameters D, k_r, λ, and λ^* were estimated by fitting the analytical solution Eq. (7) to the experimental *E. coli* breakthrough concentrations using the values of ρ θ U, and k_c listed in Table 1. Furthermore, it was assumed that $\lambda^*=\lambda/2$ (Sim and Chrysikopoulos, 1996) so that the number of fitted parameters is reduced to three, because fitting more than three parameters does not lead to reliable and unique estimates.

Fig. 5 presents the normalized MS2 breakthrough data together with the fitted model predictions. The parameters D, k_r, λ, and λ^* were estimated by fitting the analytical solution Eq. (7) to the experimental MS2 breakthrough concentrations using the values of ρ θ U, and k_c listed in Table 1. Furthermore, it was assumed that $\lambda^*=\lambda/2$ (Sim and Chrysikopoulos, 1996) so that the number of fitted parameters is reduced to three, because fitting more than three parameters does not lead to reliable and unique estimates. The fitted k_r values were negligible, the fitted λ ranged between 0.0000 and 0.0004 min^{-1}, and the fitted D values are listed in Table 1. With the exception of the

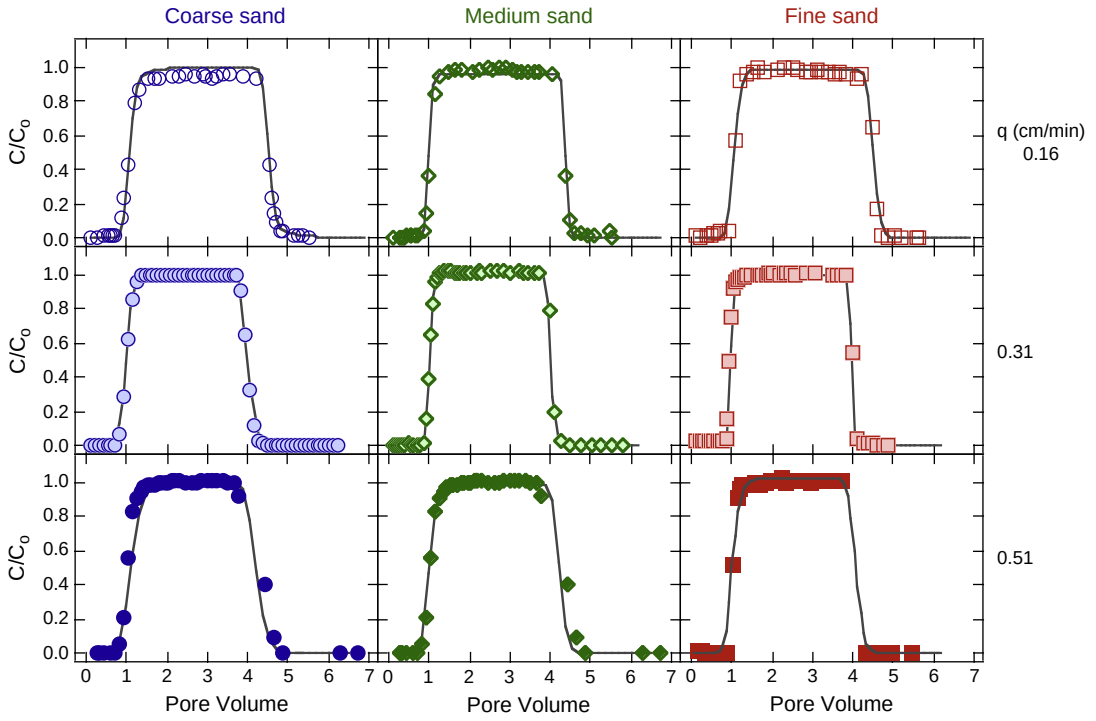

Fig. 4. Experimental *E. coli* CN13 breakthrough data (symbols) and fitted mathematical model predictions (solid curves) for volumetric flow rates of 0.16 cm/min (open symbols), 0.31 cm/min (filed symbols), and 0.51 cm/min (solid symbols) in water-saturated columns packed with coarse (circles), medium (diamonds) and fine (squares) sand.

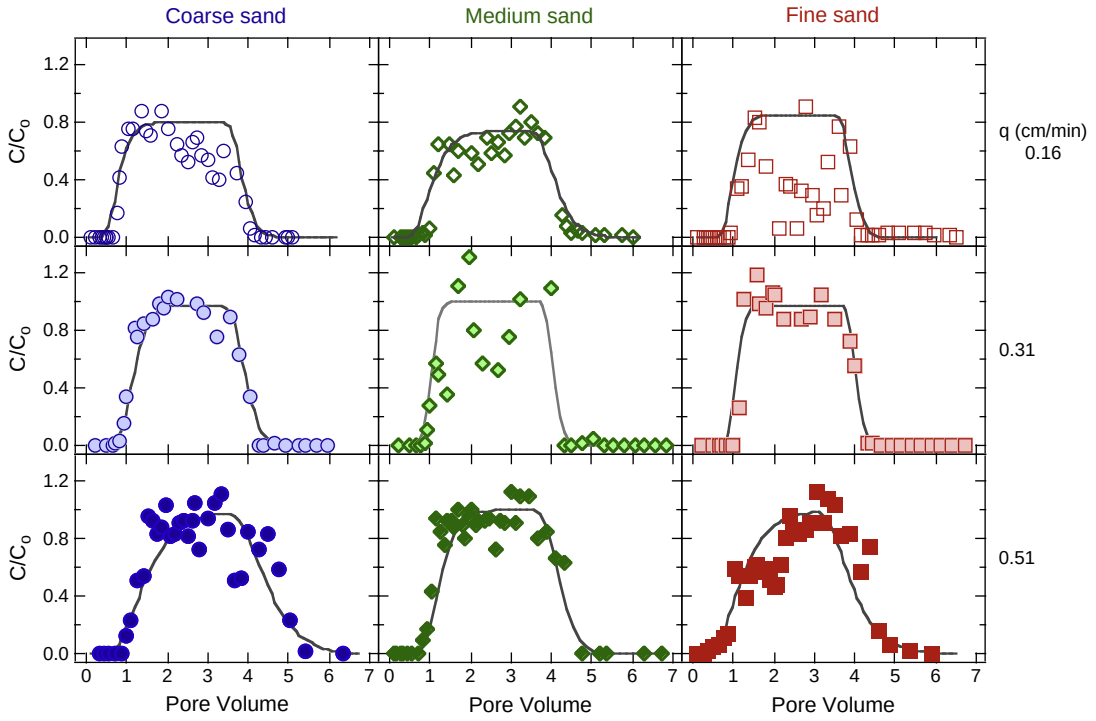

Fig. 5. Experimental MS2 breakthrough data (symbols) and fitted mathematical model predictions (solid curves) for volumetric flow rates of 0.16 cm/min (open symbols), 0.31 cm/min (filed symbols), and 0.51 cm/min (solid symbols) in water-saturated columns packed with coarse (circles), medium (diamonds) and fine (squares) sand.

case of fine sand at q = 0.51 cm/min, all estimated M_r values listed in Table 1 were quite low. Certainly, MS2 attachment and inactivation could have contributed to the observed low M_r values. For the slowest specific discharge velocity (q = 0.16 cm/min) M_r decreased with decreasing sand size; however, for the other two velocities employed there was no clear trend. Hence, the observed increase in MS2 retention cannot be attributed to d_c variations, but to possible sand grain physicochemical heterogeneities (near-neutrally charged hydrophobic regions, metal oxide impurities (e.g., Al_2O_3 and Fe_2O_3) and surface bound contaminants (e.g. organic molecules)). With the exception of the case of medium sand with q = 0.31 cm/min, where slight retardation was observed ($M_{1(i)}/M_{1(t)} = 1.05 > 1$), all calculated $M_{1(i)}/M_{1(t)}$ ratios were smaller than one (see Table 1), suggesting that the velocity of MS2 is enhanced by 2%–19% compared to the tracer.

Fig. 6 shows the normalized ΦX174 breakthrough data together with the fitted model predictions. The parameters D, k_r, and $\lambda^* = \lambda/2$ were estimated by fitting the analytical solution Eq. (7) to the experimental ΦX174 breakthrough concentrations using the values of ρ θ U, and k_c listed in Table 1. The fitted k_r values were negligible, the fitted $\lambda = 2\lambda^*$ ranged between 0.0000 and 0.0013 min^{-1}, and the fitted D values are listed in Table 1. The calculated M_r values listed in Table 1 indicated that there was no significant ΦX174 retention in the packed column. Furthermore, all calculated $M_{1(i)}/M_{1(t)}$ ratios were smaller than one (see Table 1), suggesting that the velocity of ΦX174 is enhanced by 4%–18% compared to the tracer. However, it should be noted that no clear trends between M_r or $M_{1(i)}/M_{1(t)}$ and q or d_c could be determined from the data listed in Table 1. Although the inactivation rates for coliphages used are relatively small, MS2 inactivation is more than two times larger than that of ΦX174. Therefore, the difference in inactivation rate coefficients contributes to less MS2 breakthrough than ΦX174.

The mean α_L values for each sand grain size listed in Table 1 were smaller for bacteria (*E. coli*) than coliphages (MS2, ΦX174), but higher for MS2 than ΦX174. The observed differences between the mean α_L values of MS2 and ΦX174 are attributed mainly to the different protein coats (hydrophobic for MS2 and hydrophilic for ΦX174). Furthermore, the observed differences between the mean α_L values of bacteria and coliphages are attributed to the size difference (the d_p of *E. coli* is approximately two orders of magnitude larger than that of MS2 and ΦX174). The dispersivity of colloids is known to decrease with increasing particle size (Keller et al., 2004; Vasiliadou and Chrysikopoulos, 2011). Worthy to note is that the M_r of ΦX174 was higher than that of MS2 for all cases examined in this study. MS2 generally exhibits poorer attachment to solid surfaces (Jin et al., 1997), and ΦX174 is less negatively charged than MS2 at the experimental conditions of this study. Therefore, ΦX174 is expected to attach more than MS2. Instead, a greater amount of MS2 was retained than ΦX174.

The higher attachment observed for MS2 compared to ΦX174 is also attributed to protein coat differences (the protein coat of MS2 is hydrophobic and the protein coat of

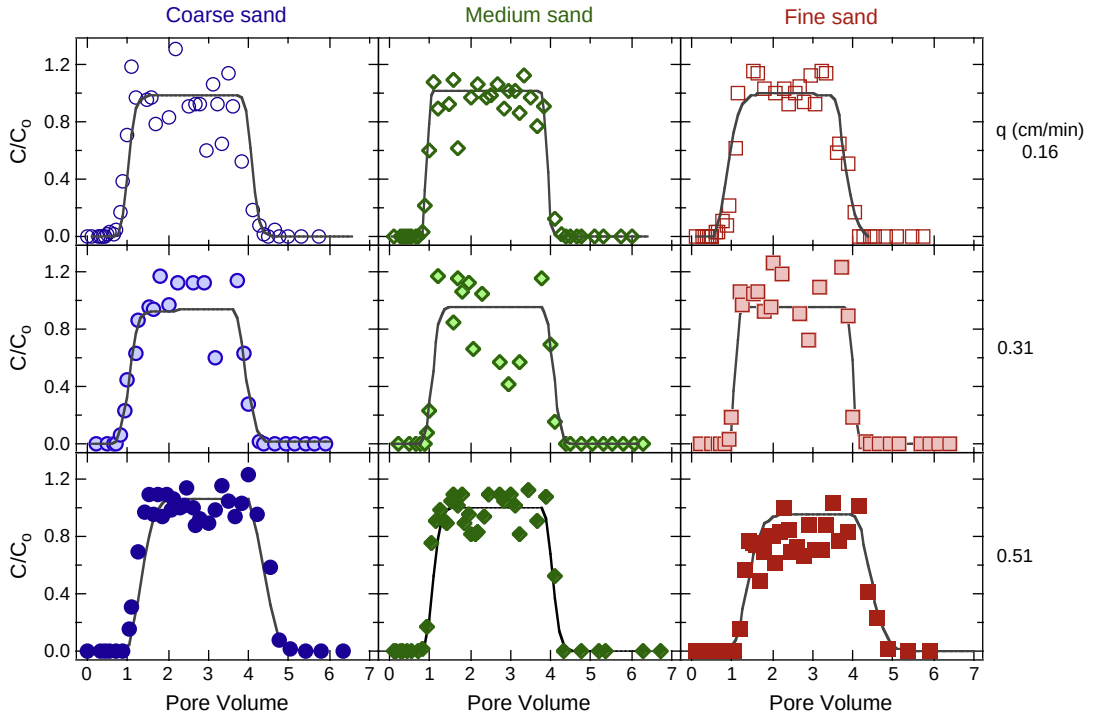

Fig. 6. Experimental ΦX174 breakthrough data (symbols) and fitted mathematical model predictions (solid curves) for volumetric flow rates of 0.16 cm/min (open symbols), 0.31 cm/min (filed symbols), and 0.51 cm/min (solid symbols) in water-saturated columns packed with coarse (circles), medium (diamonds) and fine (squares) sand.

Table 2
Parameter values used for η_0, α, and k_c calculations.

Parameter	Value (units)
Column length	0.3 (m)
Column diameter	0.025 (m)
Sand diameter (d_c)	
Coarse	1.41 (mm)
Medium	0.513 (mm)
Fine	0.181 (mm)
Particle diameter (d_p)	
MS2	0.025 (μm)
ΦX174	0.026 (μm)
E. coli	1.21 (μm)
Particle density (ρ_p)	
MS2	1420 (kg/m^3)
ΦX174	1600 (kg/m^3)
E. coli	1080 (kg/m^3)
Fluid absolute temperature (T)	298 (K)
Fluid density (ρ_f)	999.7 (kg/m^3)
Fluid viscosity (μ)	8.91×10^{-4} (kg/(m·s))
Complex Hamaker constant (A_{123})	7.5×10^{-21}(J)
Boltzman constant (k_B)	1.38×10^{-23} (kg m^2)/(s^2 K)

ΦX174 is hydrophilic (Shields, 1986)). Furthermore, the retention of coliphages was greater than that of bacteria, suggesting that deposition is smaller for larger particles, which is in agreement with the results reported by other investigators (Gupta et al., 2009; Harvey and Garabedian, 1991). However, for certain experimental conditions greater removal of bacteria than viruses has been reported in the literature (Hijnen et al., 2005; van der Wielen et al., 2008). Straining (particle trapping in pore throats that are too small to allow particle passage) and wedging (particle attachment onto surfaces of two or more collector grains in contact) are not considered important mechanisms of mass loss in the packed columns examined in this study because the biocolloid to collector diameter ratios (d_p/d_c) were well below the suggested threshold of 0.004 (Johnson et al., 2010) or 0.003 (Bradford and Bettahar, 2006) for all cases examined except the case of *E. coli* with fine sand where $d_p/d_c = 0.0067$. However, other factors (e.g. collector surface heterogeneity and angularity) may have contributed to the observed biocolloid retention.

4.2. Calculation of parameter values

According to the colloid filtration theory, particle attachment is governed by the collision efficiency, α (Rajagopalan and Tien, 1976; Tufenkji and Elimelech, 2004). Fig. 7 presents the collision efficiencies, α, for MS2, ΦX174 and *E. coli* for the experimental conditions of this study, as predicted by Eq. (12) using the previously calculated η_0 values and parameter values listed in Table 2. The calculated α values (see Table 1) exhibit some variability because they depend on a variety of parameters including the nature of the grain surface (Mills et al., 1994), the ionic strength of the solution (Jewett et al., 1995), the presence of natural organic matter (Johnson and Logan, 1996), and biocolloid surface properties (Jin et al., 1997). Furthermore, the α values calculated in this study (see Table 1) are similar to values reported in the literature for MS2 (based on field studies: $\alpha = 0.004$ (Deborde et al., 1999), 0.0027 and 0.0046 (Anders and Chrysikopoulos, 2005), 0.00027-0.0014 (Schijven et al., 1999), and a column

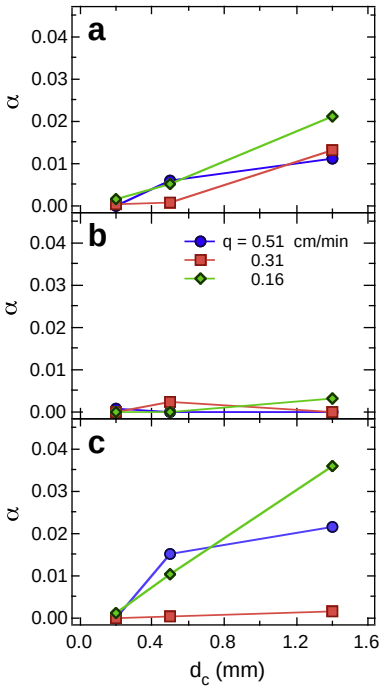

Fig. 7. Experimental collision efficiencies as a function of sand grain size and specific discharge velocity for (a) MS2, (b) ΦX174, and (c) *E. coli*.

study: $\alpha = 0.00045$-0.0422 (Chu et al., 2003)), for ΦX174 (based on a column study: $\alpha = 0.00077$–0.0162 (Chu et al., 2003)), and for *E. coli* (based on column studies: $\alpha = 0.008$-0.875 (Foppen et al., 2007), 0.026-0.937 (Foppen and Schijven, 2005)). Fig. 7 suggests that more favorable attachment conditions existed for MS2 than for ΦX174. Although this observation is biased because the MS2 inactivation is approximately twice that of ΦX174, it is an expected result because the protein coat of MS2 is hydrophobic whereas the protein coat of ΦX174 is hydrophilic (Shields, 1986). Clearly, Fig. 7 shows that there is a dependence of the biocolloid collision efficiency on d_c, suggesting that greater amounts of biocolloids are attached onto larger than smaller sand grains. This observation is in agreement with the work by Torkzaban et al. (2007) who have reported that larger collectors have greater amounts of attachment than smaller collectors under chemically unfavorable conditions, because the drag force acting on the colloids along the collector surface decreases with increasing collector size. Worthy to note is that contradictory observations of smaller collectors associated with greater amounts of colloid retention have also been reported in the literature (Bradford et al., 2007). Although detachment rate constants and inactivation of coliphages in the laboratory-scale column experiments of this study were found to be relatively negligible due to short residence time, certainly this may not be the case for biocolloid transport at the field-scale where the detachment rate and inactivation constants of suspended and attached viruses could be significant.

The calculation of the theoretical collision efficiencies, α_{th}, required appropriate values for Φ_{max1} and Φ_{min2}, which were obtained directly from the total intersurface potential energy curves, Φ_{tot}, estimated according to the Derjaguin–Landau–

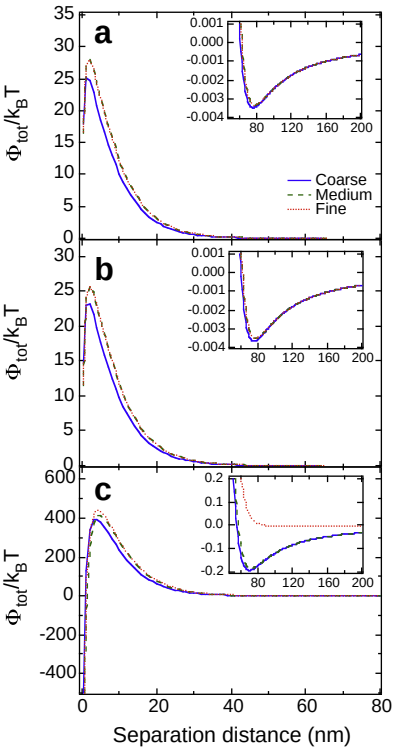

Fig. 8. Calculated total interaction energy profiles between (a) MS2, (b) ΦX174 and (c) *E. coli* and collector grain surfaces as a function of separation distance for three different sand sizes.

Verwey–Overbeek (DLVO) theory of colloid stability using Eqs. (27)–(31). The estimated Φ_{tot} profiles for MS2, ΦX174 and *E. coli* particles approaching various sand grains (coarse, medium and fine) are shown in Fig. 8. Note that when *E. coli* cells approach sand grains face an energy barrier of several 100 k_BT, while lower energy barriers of several 10 k_BT are encountered by coliphages (see Fig. 8). The estimated Φ_{max1} and Φ_{min2} values are listed in Table 3 together with the corresponding zeta potentials. In this study, biocolloids were considered to follow the principles of colloid chemistry, despite the fact that they are more complex than abiotic colloids (van Loosdrecht et al., 1989). For the Φ_{dl} calculations, the electrokinetic zeta potentials were used instead of the surface potentials. The zeta potentials of the various biocolloid particles and sand grains suspended in PBS solution were measured with a Zetameter (Malvern Instruments) following the procedure outlined by Syngouna and Chrysikopoulos (2010), and they are listed in Table 3. Note that the *E. coli* bacteria cells were treated as spherical biocolloids because electrophoretic mobilities (Delgado and Gonzalez-Caballero, 1998) and zeta potential values (Salerno et al., 2006) are not affected by colloid particle shape. Moreover, Liu et al. (2010) demonstrated that the electrophoretic mobility values for spheroidal colloids are quite similar to the values determined by using the Hückel approximation for spherical colloids.

Note that for the experimental conditions of this study the previously discussed approaches for the estimation of the theoretical collision efficiency can be applied only for *E. coli* because, based on the results of Fig. 8, MS2 and ΦX174 do not exhibit Φ_{min1} and very small Φ_{min2} depths (smaller than the average Brownian kinetic energy of 1.5 k_BT). Consequently, Fig. 9 presents the $\log(\alpha/\alpha_{th})$ values only for *E. coli* for three different q and d_c values in an attempt to provide an illustrative comparison of α_{th} estimated by IFBL (Eq. (24)), MA1 (Maxwell approximation, Eq. (32)) and MA2 (Maxwell approximation, Eq. (35)) with the experimental collision efficiencies. Clearly, the experimental collision efficiencies measured for *E. coli* are in relatively good agreement with both MA1 and MA2 predictions (within 0-2 orders of magnitude) but not with IFBL predictions. Discrepancies between α and α_{th} within 1–1.5 orders of magnitude have also been reported in the literature by other investigators (Shen et al., 2007). Note that the α_{th} calculations presented here assume that the sand and biocolloid surfaces are uniformly charged. However, it is highly probable that both the sand grains and the biocolloids exhibit some surface charge heterogeneity (Camesano and Abu-Lail, 2002; Song et al., 1994; Walker et al., 2004). The presence of hetero-domains of attractive surface charge is known to enhance colloid retention in the presence of energy barriers (Auset and Keller, 2006; Elimelech and O'Melia, 1990).

5. Summary and conclusions

A large number of column experiments were carried out in order to investigate the effects of water velocity and sand grain size on biocolloid transport. The results of this study indicated that although the biocolloid mass recovery and degree of velocity enhancement were affected by the interstitial water velocity and sand grain size, no clear trends could be determined. It was found that the dispersivity values for MS2 were higher than those obtained for ΦX174, which could be attributed to the higher charge repulsion between MS2 and sand grains (higher energy barriers) and to the hydrophobic protein coat of MS2. Moreover, as it was expected, the dispersivity values for the smaller coliphages were found to be greater than that of the larger bacteria. The single collector removal efficiency under favorable deposition conditions was shown to be affected by the sand grain size and water velocity. In general, the experimental results indicated that η_0 values increased with

Table 3
Measured zeta potentials in PBS solution (pH = 7, I_S = 2 mM), and calculated Φ_{max1} and Φ_{min2} values.

	Zeta potential (mV)	Coarse sand ($\zeta = -53.03 \pm 2.13$ mV)		Medium sand ($\zeta = -62.25 \pm 3.45$ mV)		Fine sand ($\zeta = -64.72 \pm 3.12$ mV)	
		Φ_{max1} (k_BT)	Φ_{min2} (k_BT)	Φ_{max1} (k_BT)	Φ_{min2} (k_BT)	Φ_{max1} (k_BT)	Φ_{min2} (k_BT)
MS2	-33.5 ± 1.8	25.06	−0.00349	28.09	−0.00334	27.97	−0.00335
ΦX174	-31.15 ± 0.25	23.13	−0.00368	25.83	−0.00353	25.63	−0.00353
E. coli	-18.46 ± 3.66	395.55	−0.19217	412.82	−0.18341	428.47	−0.00194

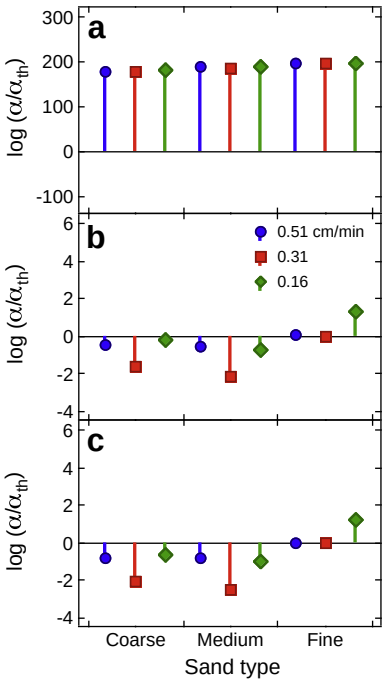

Fig. 9. Comparison between experimental and theoretical collision efficiencies for *E. coli* predicted with (a) IFBL, (b) MA1, and (c) MA2.

decreasing water velocity and sand grain size for all biocolloids examined. The experimental collision efficiencies suggested that more favorable attachment conditions existed for coliphage MS2 than for ΦX174. However no significant effect of sand grain size and interstitial velocity on the collision efficiency was observed. It is possible that factors as grain surface area, angularity and roughness may have contributed to physicochemical filtration and biocolloid retention. Theoretical collision efficiencies were calculated only for *E. coli* using both the IFBL and Maxwell approximations. For the IFBL approximation, the disagreement between observations and theory was more pronounced. To minimize the observed discrepancies, estimates of α_{th} should also account for surface heterogeneities, surface roughness, and hydrodynamic forces.

Nomenclature

A_{123}	Complex Hamaker constant for biocolloid-water-sand, $(M\,L^2)/t^2$.
A_N	Avogadro's number, 1/mol.
A_s	Porosity-dependent flow parameter, defined in Eq. (17).
C	Concentration of biocolloids in suspension, M/L^3.
C^*	Concentration of biocolloids attached on the solid matrix, M/L^3.
C_0	Source concentration of biocolloid in suspension, M/L^3.
d_c	Average collector diameter, L.
d_p	Biocolloidal particle diameter, L.
D	Hydrodynamic dispersion coefficient, L^2/t.
D	Molecular diffusion coefficient, L^2/t.
D_e	Effective molecular diffusion coefficient, L^2/t.
e	Elementary charge, C.
E_k	Kinetic energy, J.
erfc[·]	Complimentary error function.
g	Acceleration due to gravity, L/t^2.
h	Particle-collector separation distance.
i	Subscript indicates *E. coli*, MS2, and ΦX174
I_s	Ionic strength, mol/L.
J_0	Bessel function of the first kind of zeroth order
k_B	Boltzman's constant, $(M\cdot L^2)/(t^2K)$.
k_c	Attachment rate constant, t^{-1}.
k_r	Detachment rate constant, t^{-1}.
L	Length of the porous medium, L.
m_n	nth absolute temporal moment, defined in Eq. (9), t^n.
M_n	nth normalized temporal moment, defined in Eq. (10), t^n.
m_p	Mass of a particle, M.
M_r	Mass recovery, defined in Eq. (11).
n	Subscript indicating the order of the moment.
N_A	Attraction number, defined in Eq. (21).
N_G	Gravity number, defined in Eq. (22).
N_{Pe}	Peclet number, defined in Eq. (19).
N_R	Relative size number, defined in Eq. (18).
N_{vdW}	Van der Waals number, defined in Eq. (20).
q	Specific discharge or approach velocity, L/t.
Q	Volumetric discharge rate, L^3/t.
r_c	Average collector radius, L.
r_p	Average biocolloidal particle diameter, L.
RB	Normalized mass recovery, defined in Eq. (13)
$S(\beta)$	Function describing the collection of Brownian particles onto a collector, (−).
t	Time, t.
t_p	Duration of the solute pulse, t.
T	Temperature, Kelvin.
U	Interstitial (pore water flow) velocity, L/t.
v_p	Particle velocity in the secondary minimum, L/t.
x	Spatial coordinate in the horizontal direction, L.
α	Collision efficiency, (−).
α_{th}	Theoretical collision efficiency, (−).
α_L	Longitudinal dispersivity, L/t.
β	Dimensionless sticking parameter, defined in Eq. (25).
Γ	Gamma function
ε	Dielectric constant of the suspending liquid, $C^2/(J\cdot m)$.
ε_r	Relative dielectric constant of the suspending liquid, (−).
ε_0	Permittivity of free space, $C^2/(J\cdot m)$.
ε_θ	Equal to $(1-\theta)^{1/3}$
ζ	Electrokinetic zeta potentials of the particles and sand grains, V.
η_0	Single-collector removal efficiency for favorable deposition, (−).
θ	Porosity of soil (liquid volume/porous medium volume), L^3/L^3.
κ	Debye–Huckel parameter, 1/L.
λ	Transformation rate constant of biocolloids in solution, t^{-1}.
λ^*	Transformation rate constant of attached biocolloids, t^{-1}.
λ_β	Surface reaction rate coefficient describing adhesion, defined in Eq. (26).
λ_w	Characteristic wavelength of the sphere-plate interaction, L.
μ_w	Water viscosity, $M/(L\cdot t)$.
ξ	Dummy integration variable.

ρ	Bulk density of the solid matrix (solids mass/aquifer volume), M/L^3.
ρ_f	Density of the fluid, M/L^3.
ρ_p	Biocolloidal particle density, M/L^3.
σ	Born collision parameter, L.
τ	Dummy integration variable.
τ^*	Tortuosity (–).
Φ_{Born}	Born potential energy, J.
Φ_{dl}	Double layer potential energy, J.
Φ_{max1}	Primary maximum of Φ_{tot}, J.
Φ_{min1}	Primary minimum of Φ_{tot}, J.
Φ_{min2},	Secondary minimum of Φ_{tot}, J.
Φ_{tot}	Total intersurface potential energy, J.
Φ_{vdW}	Van der Waals potential energy, J.
Ψ_c	Surface potential of the collector (sand), V.
Ψ_p	Surface potential of the particle, V.

Acknowledgments

This research has been co-financed by the European Union (European Social Fund-ESF) and Greek national funds through the Operational program "Education and Lifelong Learning" of the National Strategic Reference Framework (NSRF)-Research Funding Program: Heracleitus II. Investing in knowledge society through the European Social Fund.

References

Abdel-Salam, A., Chrysikopoulos, C.V., 1995. Modeling of colloid and colloid-facilitated contaminant transport in a two-dimensional fracture with spatially variable aperture. Transport in Porous Media 20, 197–221.

Adams, M.H., 1959. Bacteriophages. Interscience, New York, N.Y., pp. 450–454.

Anders, R., Chrysikopoulos, C.V., 2005. Virus fate and transport during artificial recharge with recycled water. Water Resources Research 41, W10415. doi:10.1029/2004WR003419.

Anders, R., Chrysikopoulos, C.V., 2006. Evaluation of the factors controlling the time-dependent inactivation rate coefficients of bacteriophage MS2 and PRD1. Environmental Science and Technology 40, 3237–3242.

Anders, R., Chrysikopoulos, C.V., 2009. Transport of viruses through saturated and unsaturated columns packed with sand. Transport in Porous Media 76, 121–138.

Auset, M., Keller, A., 2006. Pore-scale visualization of colloid straining and filtration in saturated porous media using micromodels. Water Resources Research 42, W12S02. doi:10.1029/2005WR004639.

Banks, M.K., Yu, W., Govindaraju, R.S., 2003. Bacterial adsorption and transport in saturated soil columns. Journal of Environmental Science and Health Part A 38, 2749–2758.

Bear, J., 1979. Hydraulics of Groundwater. McGraw-Hill.

Black, C.A. (Ed.), 1965. Methods of Soil Analysis. Part 2. Chemical and Microbiological Properties. American Society of Agronomy, Madison.

Bolster, C.H., Mills, A.L., Hornberger, G.M., Herman, J.S., 2001. Effect of surface coatings, grain size, and ionic strength on the maximum attainable coverage of bacteria on sand surfaces. Journal of Contaminant Hydrology 50, 287–305.

Bradford, S.A., Bettahar, M., 2006. Concentration dependent transport of colloids in saturated porous media. Journal of Contaminant Hydrology 82, 99–117.

Bradford, S.A., Torkzaban, S., Walker, S.L., 2007. Coupling of physical and chemical mechanisms of colloid straining in saturated porous media. Water Research 41, 3012–3024.

Bueche, F.J., 1975. Introduction to physics for scientists and engineers, 2nd Edition. McGraw-Hill, p. 870.

Camesano, T.A., Abu-Lail, N.I., 2002. Heterogeneity in bacterial surface polysaccharides, probed on a single-molecule basis. Biomacromolecules 3, 661–667.

Chrysikopoulos, C.V., 1993. Artificial tracers for geothermal reservoir studies. Environmental Geology 22, 60–70.

Chrysikopoulos, C.V., Sim, Y., 1996. One-dimensional virus transport homogeneous porous media with time dependent distribution coefficient. Journal of Hydrology 185, 199–219.

Chrysikopoulos, C.V., Masciopinto, C., La Mantia, R., Manariotis, I.D., 2010. Removal of biocolloids suspended in reclaimed wastewater by injection in a fractured aquifer model. Environmental Science and Technology 44, 971–977.

Chu, Y., Jin, Y., Baumann, T., Yates, M.V., 2003. Effect of soil properties on saturated and unsaturated virus transport through columns. Journal of Environmental Quality 32, 2017–2025.

Dahneke, B., 1975. Resuspension of Particles. Journal of Colloid and Interface Science 50, 194–196.

Deborde, D.C., Woessner, W.W., Kiley, Q.T., Ball, P., 1999. Rapid transport of viruses in a floodplain aquifer. Water Research 33, 2229–2238.

Delgado, A.V., Gonzalez-Caballero, F., 1998. Inorganic particles as colloidal modela. Effects of size and shape on the electrokinetics of hematite (a-Fe_2O_3). Croatica Chemica Acta 71, 1087–1104.

Elimelech, M., O'Melia, C.R., 1990. Effect of particle size on collision etliciency in the deposition of Brownian particles with electrostatic energy barriers. Langmuir 6, 1153–1163.

Feng, H., Yu, Z., Chu, P.K., 2006. Materials Science and Engineering Reports 54, 49–120.

Foppen, J.W.A., Schijven, J.F., 2005. Transport of *E. coli* in columns of geochemically heterogeneous sediment. Water Research 39, 3082–3088.

Foppen, J.W., van Herwerden, M., Schijven, J., 2007. Transport of *Escherichia coli* in saturated porous media: dual mode deposition and intra-population heterogeneity. Water Research 41, 1743–1753.

Gregory, J., 1981. Approximate expressions for retarded van der Waals interaction. Journal of Colloid and Interface Science 83, 138–145.

Gupta, V., Johnson, W.P., Shafieian, P., Ryu, H., Alum, A., Abbaszadegan, M., Hubbs, S.A., Rauch-Williams, T., 2009. Riverbank filtration: Comparison of Pilot Scale Transport with Theory. Environmental Science and Technology 43, 669–676.

Hahn, M.W., O'Melia, C.R., 2004. Deposition and reentrainment of Brownian particles in porous media under unfavorable chemical conditions: some concepts and applications. Environmental Science and Technology 38, 210–220.

Harvey, R.W., Garabedian, S.P., 1991. Use of colloid filtration theory in modelling movement of bacteria through a contaminated sandy aquifer. Environmental Science and Technology 25, 178–185.

Hendry, M., Lawrence, J., Maloszewski, P., 1999. Effects of velocity on the transport of two bacteria through saturated sand. Ground Water 37, 103–112.

Hijnen, W.A., Brouwer-Hanzens, A.J., Charles, K.J., Medema, G.J., 2005. Transport of MS2 phage, *Escherichia coli*, *Clostridium perfringens*, *Cryptosporidium parvum*, and *Giardia intestinalis* in a gravel and a sandy soil. Environmental Science and Technology 39, 7860–7868.

Hogg, R., Healy, T.W., Fuerstenau, D.W., 1966. Mutual coagulation of colloidal dispersions. Transactions of the Faraday Society 62, 1638–1651.

James, S.C., Chrysikopoulos, C.V., 2011. Monodisperse and polydisperse colloid transport in water-saturated fractures with various orientations: gravity effects. Advances in Water Resources 34, 1249–1255. doi:10.1016/j.advwatres.2011.06.001.

Jewett, D.G., Hilbert, T.A., Logan, B.E., Arnold, R.G., Bales, R.C., 1995. Bacterial transport in laboratory columns and filters: influence of ionic strength and pH on collision efficiency. Water Research 29, 1673–1680.

Jin, Y., Yates, M.V., Thompson, S.S., Jury, W.A., 1997. Sorption of viruses during flow through saturated sand columns. Environmental Science and Technology 31, 548–555.

Johnson, W.P., Logan, B.E., 1996. Enhanced transport of bacteria in porous media by sediment-phase and aqueous-phase natural organic matter. Water Research 30, 923–931.

Johnson, W.P., Pazmino, E., Ma, H., 2010. Direct observations of colloid retention in granular media in the presence of energy barriers, and implications for inferred mechanisms from indirect observations. Water Research 44, 1158–1169.

Keller, A.A., Sirivithayapakorn, S., Chrysikopoulos, C.V., 2004. Early breakthrough of colloids and bacteriophage MS2 in a water saturated sand column. Water Resources Research 40, W08304 doi:1029/2003WR002676.

Klaus, D., Simske, S., Todd, P., Stodieck, L., 1997. Investigation of space flight effects on Escherichia coli and a proposed model of underlying physical mechanisms. Microbiology 143, 449–455.

Liu, Q., Lazouskaya, V., He, Q., Jin, Y., 2010. Effect of Particle Shape on Colloid Retention and Release in Saturated Porous Media. Journal of Environmental Quality 39, 500–508.

Loveland, J.P., Ryan, J.N., Amy, G.L., Harvey, R.W., 1996. The reversibility of virus attachment to mineral surfaces. Colloids and Surfaces A: Physicochemical and Engineering Aspects 107, 205–221.

Maki, N., Gestwicki, J.E., Lake, E.M., Kiessling, L.L., Adler, J., 2000. Motility and chemotaxis of filamentous cells of *Escherichia coli*. Journal of Bacteriology 182, 4337–4342.

Masciopinto, C., La Mantia, R., Chrysikopoulos, C.V., 2008. Fate and transport of pathogens in a fractured aquifer in the Salento area, Italy. Water Resources Research 44, W01404. doi:10.1029/2006WR005643.

Mills, A.L., Herman, J.S., Hornberger, G.M., De Jesús, T.H., 1994. Effect of solution ionic strength and iron coatings on minerals grains on the sorption of bacterial cells to quartz sand. Applied and Environmental Microbiology 60, 3300–3306.

Murray, J.P., Parks, G.A., 1978. Particulates in water: characterization, fate, effects and removal. In: Kavanaugh, M.C., Leckie, J.O. (Eds.), Adv. Chem. Ser., 189. American Chemical Society, Washington, DC.

Rajagopalan, R., Tien, C., 1976. Trajectory analysis of deep-bed filtration with the sphere-in-cell porous media model. AICHE Journal 22, 523–533.

Robinson, R.A., Stokes, R.H., 1959. Electrolyte solutions, The Measurement and Interpretation of Conductance, Chemical Potential and Diffusion in Solutions of Simple Electrolytes, 2nd ed. Butterworths, London, p. 559.

Ruckenstein, E., Prieve, D.C., 1976. Adsorption and desorption of particles and their chromatographic separation. AICHE Journal 22, 276–283.

Ryan, J.N., Elimelech, M., Ard, R.A., Harvey, R.W., Johnson, P.R., 1999. Bacteriophage PRD1 and silica colloid transport and recovery in an iron oxide-coated sand aquifer. Environmental Science and Technology 33, 63–73.

Sadeghi, G., Schijven, J.F., Behrends, T., Hassanizadeh, S.M., Gerritse, J., Kleingeld, P.J., 2011. Systematic study of effects of pH and ionic stregth on attachment of phage PRD1. Ground Water 49 (1), 12–19.

Salerno, M.B., Flamm, M., Logan, B.E., Velegol, D., 2006. Transport of rod-like colloids through packed beds. Environmental Science and Technology 40, 6336–6340.

Schijven, J.F., Hoogenboezem, W., Hassanizadeh, S.M., Peters, J.H., 1999. Modeling removal of bacteriophages MS2 and PRD1 by dune recharge at Castricum, Netherlands. Water Resources Research 35, 1101–1111.

Shen, C., Li, B., Huang, Y., Jin, Y., 2007. Kinetics of coupled primary- and secondary-minimum deposition of colloids under unfavorable chemical conditions. Environmental Science and Technology 41, 6976–6982.

Shields, P.A., 1986. Factors inffuencing virus adsorption to solids. Ph.D. Dissertation, University of Florida, Gainesville, FL.

Sim, Y., Chrysikopoulos, C.V., 1995. Analytical models for one-dimensional virus transport in saturated porous media. Water Resources Research 31, 1429–1437 (Correction, Water Resour. Res., 32, 1473, 1996).

Sim, Y., Chrysikopoulos, C.V., 1996. One-dimensional virus transport in porous media with time dependent inactivation rate coefficients. Water Resources Research 32 (8), 2607–2611.

Sim, Y., Chrysikopoulos, C.V., 1998. Three-dimensional analytical models for virus transport in saturated porous media. Transport in Porous Media 30, 87–112.

Sim, Y., Chrysikopoulos, C.V., 1999. Analytical solutions for solute transport in saturated porous media with semi-infinite or finite thickness. Advances in Water Resources 22, 507–519.

Sim, Y., Chrysikopoulos, C.V., 2000. Virus transport in unsaturated porous media. Water Resources Research 36, 173–179.

Simoni, S.F., Harms, H., Bosma, T.P., Zehnder, A.J., 1998. Population heterogeneity affects transport of bacteria through sand columns at low flow rates. Environmental Science and Technology 32, 2100–2105.

Sinton, L.W., Noonan, M.J., Finlay, R.K., Pang, L., Close, M.E., 2000. Transport and attenuation of bacteria and bacteriophage in an alluvial gravel aquifer. New Zealand Journal of Marine and Freshwater Research 34, 175–186.

Song, L.F., Johnson, P.R., Elimelech, M., 1994. Kinetics of colloid deposition onto heterogeneously charged surfaces in porous media. Environmental Science and Technology 28, 1164–1171.

Spielman, L.A., Friedlander, S.K., 1974. Role of electric double layer in particle deposition by convective diffusion. Journal of Colloid and Interface Science 46, 22–31.

Syngouna, V.I., Chrysikopoulos, C.V., 2010. Interaction between viruses and clays in static and dynamic batch systems. Environmental Science and Technology 44, 4539–4544.

Tong, M., Johnson, W.P., 2007. Colloid population heterogeneity drives hyper-exponential deviation from classic filtration theory. Environmental Science and Technology 41, 493–499.

Torkzaban, S., Bradford, S.A., Walker, S.L., 2007. Resolving the coupled effects of hydrodynamics and DLVO forces on colloid attachment to porous media. Langmuir 23, 9652–9660.

Torkzaban, S., Bradford, S.A., van Genuchten, M.Th., Walker, S.L., 2008. Colloid transport in unsaturated porous media: the role of water content and ionic strength on particle straining. Journal of Contaminant Hydrology 96, 113–127.

Tufenkji, N., Elimelech, M., 2004. Correlation equation for predicting single-collector efficiency in physicochemical filtration in saturated porous media. Environmental Science and Technology 38, 529–536.

van der Wielen, P.W.J.J., Senden, W.J.M.K., Medema, G., 2008. Removal of bacteriophages MS2 and ΦX174 during transport in a sandy anoxic aquifer. Environmental Science and Technology 42, 4589–4594.

van Loosdrecht, M.C.M., Lyklema, J., Norde, W., Zehnder, A.J.B., 1989. Bacterial adhesion: a physicochemical approach. Microbial Ecology 17, 1–15.

Vasiliadou, I.A., Chrysikopoulos, C.V., 2011. Cotransport of *Pseudomonas putida* and kaolinite particles through water saturated columns packed with glass beads. Water Resources Research 47, W02543. doi:10.1029/2010WR009560.

Vasiliadou, I.A., Papoulis, D., Chrysikopoulos, C.V., Panagiotaras, D., Karakosta, E., Fardis, M., Papavassiliou, G., 2011. Attachment of *Pseudomonas putida* onto differently structured kaolinite minerals: A combined ATR-FTIR and ^{1}H NMR study. Colloids and Surfaces B: Biointerfaces 84 (2), 354–359.

Walker, S.L., Redman, J.A., Elimelech, M., 2004. Role of cell surface lipopolysaccharides (LPS) in *Escherichia coli* K12 adhesion and transport. Langmuir 20, 7736–7746.

Walshe, G.E., Pang, L., Flury, M., Close, M.E., Flintoft, M., 2010. Effects of pH, ionic strength, dissolved organic matter, and flow rate on the co-transport of MS2 bacteriophages with kaolinite in gravel aquifer media. Water Research 44, 1255–1269.